PNAS RESEARCH ARTICLE | BIOPHYSICS AND COMPUTATIONAL BIOLOGY

# Tube feet dynamics drive adaptation in sea star locomotion

Amandine Deridoux[a,b], Sina Heydari[c,d], Stanislav. N. Gorb[e], Eva Kanso[f,1], Patrick Flammang[b], and Sylvain Gabriele[a,1]

Affiliations are included on p. 10.

Edited by David Weitz, Harvard University, Cambridge, MA; received April 28, 2025; accepted December 2, 2025

**Sea stars use hundreds of tube feet on their oral surface to crawl, climb, and navigate complex environments, despite lacking a central brain. While tube foot morphology and function as muscular hydrostats are well described, the mechanisms that coordinate their collective dynamics remain poorly understood. To investigate these dynamics, we employed an optical imaging method based on frustrated total internal reflection (FTIR) to visualize and quantify tube foot adhesive contacts in real time in the species *Asterias rubens* across individuals spanning a wide size range. Our results reveal an inverse relationship between crawling speed and tube foot adhesion time, indicating that sea stars regulate locomotion by modulating contact duration in response to mechanical load. To test this, we conducted perturbation experiments using 3D-printed backpacks that increased body mass by 25 and 50%, along with biomechanical modeling of decentralized feedback control of the tube feet. The added load significantly increased adhesion time, supporting the role of a load-dependent mechanical adaptation. We further investigated inverted locomotion, both experimentally and through simulation, and found that tube feet adjust their contact behavior when the animal is oriented upside down relative to gravity. Together, these findings demonstrate that sea stars adapt their locomotion to changing mechanical demands by modulating tube foot–substrate interactions, revealing a robust decentralized control strategy in a brainless organism and highlighting general principles of distributed control in biology and soft robotics.**

locomotion | sea star | tube foot | adhesion

## Significance

Sea stars coordinate hundreds of flexible tube feet to crawl efficiently despite lacking a centralized nervous system. This study reveals how sea stars dynamically adjust the duration of tube foot adhesion to maintain efficient crawling under varying mechanical demands, such as increased body mass or inverted posture. Using FTIR-based imaging, we quantified adhesion and detachment dynamics of individual tube feet under different mechanical conditions and combined these measurements with a biomechanical model assuming fully decentralized control. We show that locomotion emerges from local mechanical feedback: Tube feet autonomously adjust their adhesion time without any central coordination. This work uncovers a distributed control strategy in a brainless organism and identifies general principles of adaptive movement relevant to soft and multicontact robotics.

Sea stars are found in diverse marine environments, from shallow tide pools to the deeper waters of the continental shelf, where they use hundreds of flexible tube feet for foraging, posture maintenance, and attachment to the substrate. These behaviors rely on their ability to maintain their oral surface in contact with the substratum (1), allowing them to navigate and adapt to their environments (2). A critical component enabling these functions is the coordinated action of tube feet, which are specialized locomotory and adhesive appendages. Although tube feet have been well characterized morphologically and mechanically (3–5), the mechanisms by which their collective action gives rise to coordinated and adaptive locomotion remain unclear. This raises a fundamental question: Is the coordination of tube feet primarily orchestrated by a central pattern generator, or does it emerge from decentralized control and passive biomechanical coupling among the feet through the body of the sea star?

To address this question, we combined empirical observations in live sea stars with biomechanical modeling of tube foot mechanics and adhesion dynamics. This integrative approach reveals how local mechanical feedback allows individual tube feet to autonomously adjust their adhesion duration, enabling the animal to maintain efficient crawling under varying mechanical demands such as increased body mass or inverted posture.

Tube feet consist of a flexible stem with an enlarged, flattened disc at the tip. Proximally, they are connected to an internal ampulla, a small muscular sac (1, 3). Adhesion is mediated by the disc, which conforms to the substrate topography due to its viscoelastic properties (6), and by the secretion of a proteinaceous adhesive material that contributes to temporary attachment (7). This process involves a duo-gland adhesive system, in which one type of glandular cell secretes adhesive proteins, while another produces deadhesive substances to enable detachment (8–10). In the species *Asterias rubens,* the chemical composition of these adhesive secretions has been studied extensively, providing insight into the mechanisms underlying temporary adhesion (7, 11).

The stem, on the other hand, enables movement through a process powered by the water vascular system (12). This hydraulic system, filled with a fluid similar to seawater but with higher potassium concentration and osmolarity, generates the hydrostatic pressure necessary for tube foot operation (7, 10, 11). The stem of each tube foot, a hollow cylinder, provides both mobility and tensile strength (13). When internal pressure increases due to ampulla contraction, the tube foot elongates, contacts the substrate, and adheres

Author contributions: P.F. and S.G. designed research; S.G. supervised the project; A.D. performed all experiments with sea stars and analyses; S.H. and E.K. developed the theoretical model and performed simulations and analysis; A.D., P.F., and S.G. jointly discussed all experimental data and their interpretation; A.D. and S.G. analysed data and prepared the figures with S.H. and E.K.; S.N.G. contributed to experiments. The article was written by A.D. and S.G., read and corrected by all authors, who all contributed to the interpretation of the results.

The authors declare no competing interest.

This article is a PNAS Direct Submission.



[1]To whom correspondence may be addressed. Email: kanso@usc.edu or sylvain.gabriele@umons.ac.be.

This article contains supporting information online at https://www.pnas.org/lookup/suppl/doi:10.1073/pnas.2509681123/-/DCSupplemental.

Published January 13, 2026.

temporarily. The contraction of some longitudinal muscle bundles can then bend the tube foot. After detachment, muscle contraction shortens the stem, forcing the fluid back into the ampulla (1, 3). This coordinated muscle action enables the stepping movement of the tube feet (14). This movement is integral to sea star locomotion. Despite lacking a centralized nervous system (15), sea stars are capable of highly coordinated locomotion, with crawling identified as their primary mode of movement (16–20).

Across and within animal species, locomotion speed typically scales with body size or mass (21). In sea stars, locomotor capacity is expected to increase with body size, potentially due to a corresponding increase in the number and/or size of tube feet (22). Interestingly, this idea is somewhat counterintuitive: In many arthropods and climbing animals, higher locomotor speed is often associated with a reduction in the number of legs engaged in propulsion, whereas a greater number of limbs can enhance surface contact and improve adhesion when mechanical stability or attachment is prioritized (23–25). In sea stars, however, the relationship appears to vary significantly between species, underscoring the need for a more detailed understanding of tube feet dynamics (16, 22).

To advance this understanding, we focused on the dynamics of tube feet in *A. rubens*. In this species, tube feet are arranged in four rows on the oral side of each arm (2), forming a network of appendages that must act cooperatively to enable crawling. Recognizing the central role of tube feet dynamics in sea star locomotion, we developed a custom FTIR-based (frustrated total internal reflection) imaging platform to quantify adhesion and detachment events in real time. This approach overcomes a major limitation of previous studies—the difficulty of unambiguously identifying adhering tube feet—and enables automated, high-precision analysis of their attachment–detachment cycles. Finally, to interpret the experimental findings, we adapted a biomechanical model of sea star locomotion based on decentralized tube foot control (3) to examine crawling under increased weight and inverted conditions, providing further insight into the adaptive, feedback-driven strategies underlying sea star movement. In the model, tube feet are structurally coupled through their attachment to the body of the sea star but are controlled locally. Each tube foot regulates its power and recovery strokes through a feedback controller informed by local sensory input. This decentralized control architecture enables minimally coupled tube feet to self-organize into coordinated gaits that yield robust forward locomotion, closely replicating the observed sea star behavior under both standard and perturbed conditions.

## Results

**Allometric Scaling in Sea Stars.** We first investigated the scaling relationship between the body mass and the average arm length across eight sea stars species with five arms (Fig. 1*A*). The log–log displays a strong positive correlation, indicating a power-law relationship between these two parameters. The estimated slope is 0.41 (95% CI: 0.40 to 0.43), showing that arm length increases at a faster rate than body mass, consistent with positive allometry.

We then focused on the morphology of *A. rubens* (Fig. 1*B*), our model species, across a broad size range represented by 24 specimens (Fig. 1*C*). The characteristic pentaradial symmetry of *A. rubens* remains consistent over varying sizes. Fig. 1*C* further exemplifies this variability, showcasing the range of individuals analyzed in this study. To assess size-related parameters, the sea star average arm length was calculated as the mean distance from the central mouth to the tip of each of the five arms. In the log–log scale, the estimated slope was 0.36 (95% CI: 0.32 to 0.40), which encompasses the theoretical isometric scaling exponent of 0.33, indicating that arm length scales approximately isometrically with body mass in *A. rubens* (Fig. 1*D*).

To confirm the generality of these scaling relationships, we examined a second species, *Marthasterias glacialis*, also across a broad size range (*SI Appendix*, Fig. 1*A*). In this species, the estimated slope was 0.39 (95% CI of 0.35 to 0.43), suggesting a slightly positive allometry. The overlap between the CI for *A. rubens* and *M. glacialis* indicates that both species share statistically similar scaling behavior between arm length and body mass. The same positive correlation between the average arm length and the body mass was observed (*SI Appendix*, Fig. 1*B*).

We also determined the average number of tube feet per arm across the full range of sea stars with varying masses and showed it increased linearly with size and mass (Fig. 1*E*). We next examined whether the pentaradial symmetry in *A. rubens* is maintained during locomotion by labeling the arms in a clockwise manner as a, b, c, d, and e (Fig. 1*F*), using the leading arm "a" as a reference for analyzing angular arrangements. The leading arm was defined as the arm oriented in the direction of locomotion during the crawling sequence. Interestingly, the angular analysis (Fig. 1*G*) revealed a subtle asymmetry: The angle ($\gamma$) opposite to the leading arm was significantly smaller (64.9 ± 13.3°) than the others. To assess whether this asymmetry was related to individual size, we performed a two-way ANOVA including angle between arms and mass as factors. The interaction between angle between arms and mass was not significant ($P = 0.42$), confirming that the interarm asymmetry is independent of body size. However, the effect of angle between arms remained significant ($P < 0.01$), supporting that this geometrical deviation is consistently associated with locomotor orientation rather than morphological scaling.

**Quantification of the Tube Feet Dynamics.** To ensure that glass was a suitable substrate for studying sea star locomotion, we performed detachment trials using a force ramp protocol to assess adhesion capabilities (*SI Appendix*, Fig. 2 *A* and *B* and Movie 1). Additionally, we compared locomotion on glass with that on slate, a rougher, more naturalistic surface for sea stars. Crawling speed did not differ significantly between glass (0.98 ± 0.38 mm $s^{-1}$) and slate (1.12 ± 0.22 mm $s^{-1}$) surfaces (*SI Appendix*, Fig. 2*B*), even after controlling for individual body mass ($P = 0.27$) (*SI Appendix*, Fig. 2*C*), confirming that glass is an appropriate model surface for studying sea star locomotion. To visualize the contact between the tube feet of *A. rubens* and the substrate, we used a custom-built aquarium made of high-refractive-index glass ($n_1 = 1.52$) equipped with an LED strip at its base (Fig. 2 *A* and *B* and Movie 2). This setup leveraged the principle of FTIR. Under normal conditions, light traveling through the glass undergoes total internal reflection when it reaches the glass–seawater interface ($n_2 = 1.34$) at an angle exceeding the critical value, effectively "trapping" the light within the glass (Fig. 2*A*). However, when a tube foot makes close contact with the glass, it alters the local refractive index, allowing light to escape and diffuse into the second medium. This interaction illuminates the contact area, producing bright dots visible at points of adhesion (Fig. 2*C* and Movie 3).

The oral surface of the sea star was filmed using a camera positioned beneath the aquarium, allowing for precise visualization and quantification of the tube foot adhesion during locomotion. To analyze the attachment-detachment dynamics, we developed a three-step image processing and thresholding method (Fig. 2*D* and Movie 4). This method involves processing the video frames to enhance contrast, isolating the adhesion sites, and quantifying the contact area over time. This approach provided high-resolution

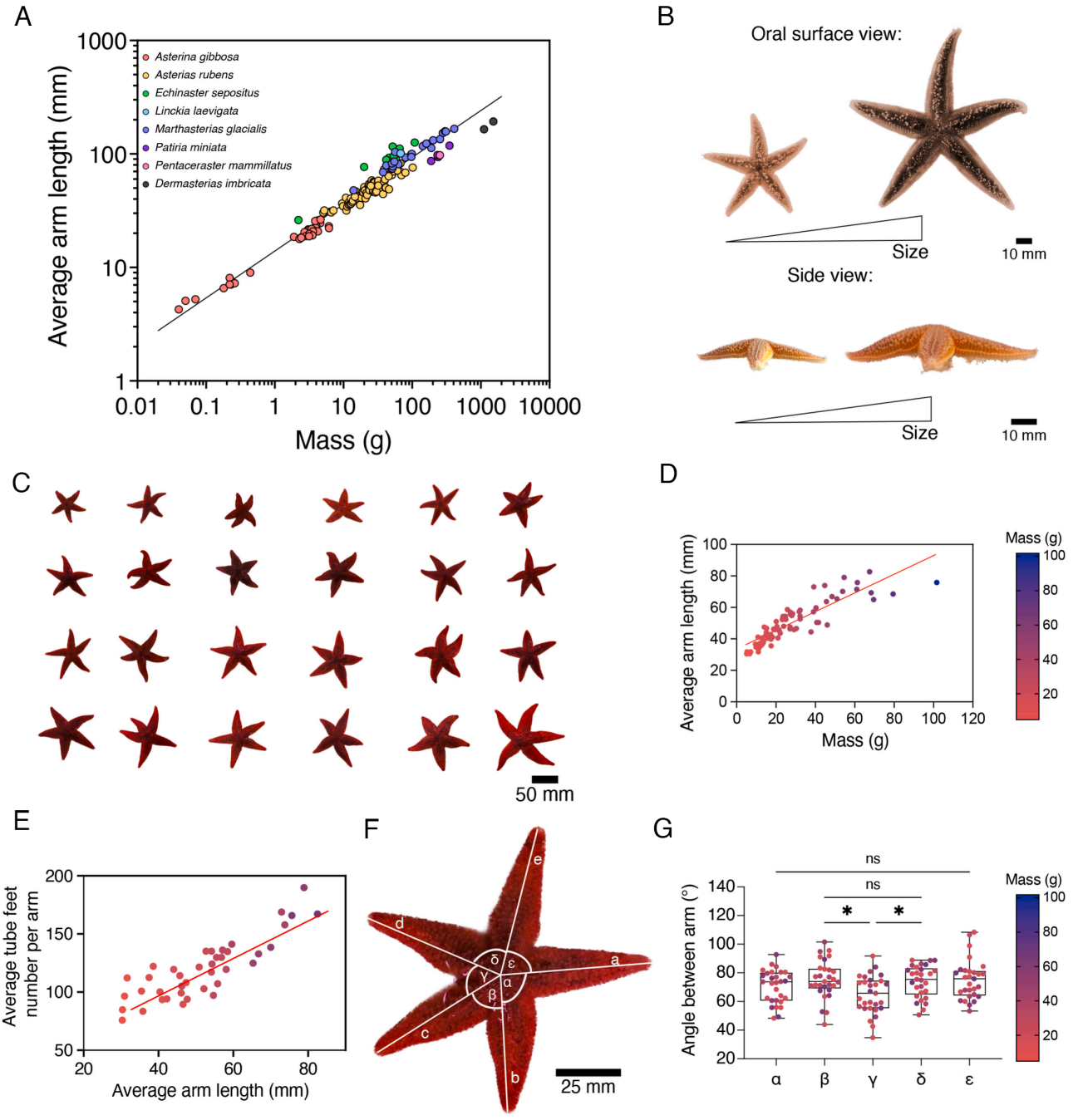


**Fig. 1.** Allometric scaling in sea stars. (*A*) Relationship between the average arm length and the sea star mass across 8 species with five arms: *Asterina gibbosa* (red, n = 37), *Echinaster sepositus* (green, n = 14), *Asterias rubens* (orange, n = 74), *Marthasterias glacialis* (blue, n = 23), *Linckia laevigata* (light blue, n = 2), *Patiria miniata* (purple, n = 4), *Dermasterias imbricata* (black, n = 2), and *Pentaceraster mammillatus* (pink, n = 1). Each dot represents one individual (n = 157 sea stars, $R^2 = 0.9541$, $P < 0.0001$). The estimated slope is 0.41 (95 % CI 0.40 to 0.43), indicating positive allometry between arm length and body mass. (*B*) Oral and lateral views of two individuals of *A. rubens* illustrating size variability. (*C*) Range of sizes observed in *A. rubens*. (Scale bar, 50 mm.) (*D*) Relationship between the body mass and the average arm length ($n = 74$, $R^2 = 0.7629$, $P < 0.0001$). (*E*) Relationship between the average tube feet number per arm and the average arm length of *A. rubens* individuals ($n = 40$, $R^2 = 0.7056$, $P < 0.0001$). (*F*) Aboral view of *A. rubens* showing labeled arms and the corresponding interarm angles. (Scale bar, 25 mm.) (*G*) Measurements of interarm angle ($n = 29$). All data are color-coded by individual mass with $^*P < 0.05$ and ns is not significant.

insights into tube foot contact behavior, offering a robust platform to study the dynamics of attachment in sea star locomotion.

**Crawling Speed in *A. rubens* Is Not Correlated With the Average Number of Tube Feet in Contact.** The locomotion of individuals of *A. rubens* was recorded over 20 s, during which the number of tube feet in contact with the substrate was dynamically monitored (Fig. 3*A*). These trials revealed that the average number of tube feet in contact (Fig. 3*B*) remained relatively constant during locomotion, with only minor fluctuations observed over time.

A significant finding from these experiments is the linear relationship between the average number of tube feet in contact and body mass both for *A. rubens* (Fig. 3*C*) and *M. glacialis* (*SI Appendix*, Fig. 3*A*). Larger individuals have an increased number of tube feet present on their oral surface, as the radius length scales with body size (Fig. 1*D*). This relationship is consistent with established scaling principles, where morphological traits tend to

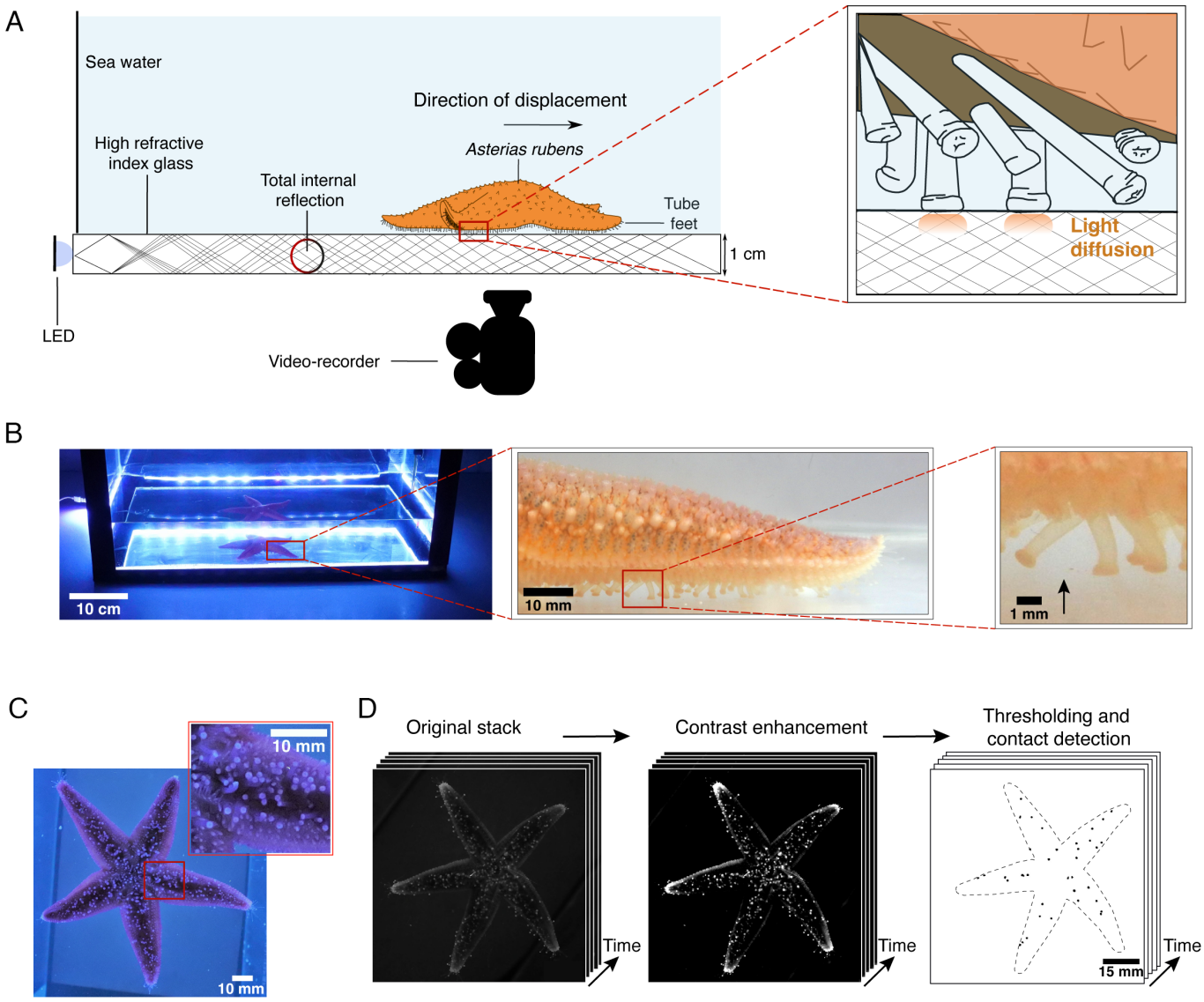


**Fig. 2.** Quantification of tube feet dynamics using FTIR-based imaging. (*A*) Schematic representation of the experimental setup, which adapts the principle of FTIR to a custom-designed aquarium. When tube feet make contact with the FTIR-equipped glass surface, they disrupt the total internal reflection, causing light to scatter and locally illuminate the contact area. Sea stars are allowed to move freely, and their movements are recorded from below using a camera positioned beneath the tank. (*B*) Photograph of the experimental setup showing the aquarium equipped with an FTIR-based imaging system. The inset provides a close-up view of an *A. rubens* arm, where contact points of individual tube feet with the substrate are clearly visible during locomotion (arrow). (*C*) Image of the oral surface of *A. rubens* crawling within the experimental setup. (*D*) Image analysis pipeline developed to quantify the number of adhering tube feet and their contact area over time from image sequences. The method includes contrast enhancement, thresholding, and automated detection for accurate temporal tracking.

increase with body mass (13). Interestingly, no significant relationship was found between crawling speed and the average number of tube feet in contact with the substrate in either *A. rubens* (Fig. 3*D*) or *M. glacialis* (*SI Appendix*, Fig. 3*B*). However, the proportion of tube feet in contact increased slightly but significantly with body mass (Fig. 3*E* and *SI Appendix*, Fig. 4*A*), indicating that larger individuals engage a somewhat higher fraction of their podia during crawling (although still < 10 %). A similar trend was observed for the total contact area (*SI Appendix*, Fig. 4*B*). Although this increase represents only a few percents of the total number of tube feet, it is statistically significant and consistent with a modest load-dependent recruitment of additional podia. This modest adjustment does not affect overall crawling speed (Fig. 3*F*), suggesting that locomotor efficiency is primarily maintained through adjustments in adhesion dynamics rather than the number of feet in contact.

**Tube Foot Adhesion Time Drives Adaptive and Efficient Sea Star Locomotion.** To further investigate adhesion dynamics, high-magnification videos of the ambulacral groove and side views videos were recorded. These recordings provided detailed visualizations of tube feet dynamics, revealing three distinct stages (Fig. 4*A* and Movie 5). The locomotion cycle begins with the attachment stage, during which the tube foot approaches the substrate at an angle, resulting in an elliptical contact shape and a circularity index less than one. This is followed by the adhesion stage, where the tube foot remains firmly attached to the substrate, referred to as the adhesion time, characterized by a circularity index close to one, reflecting a near-perfect contact. Finally, in the detachment stage, the tube foot releases from the substrate in preparation for the next movement cycle. Temporal variations in the circularity index reveal therefore fluctuating patterns that allow precise determination of the period corresponding to the adhesion time of each individual tube foot (Fig. 4*B*).

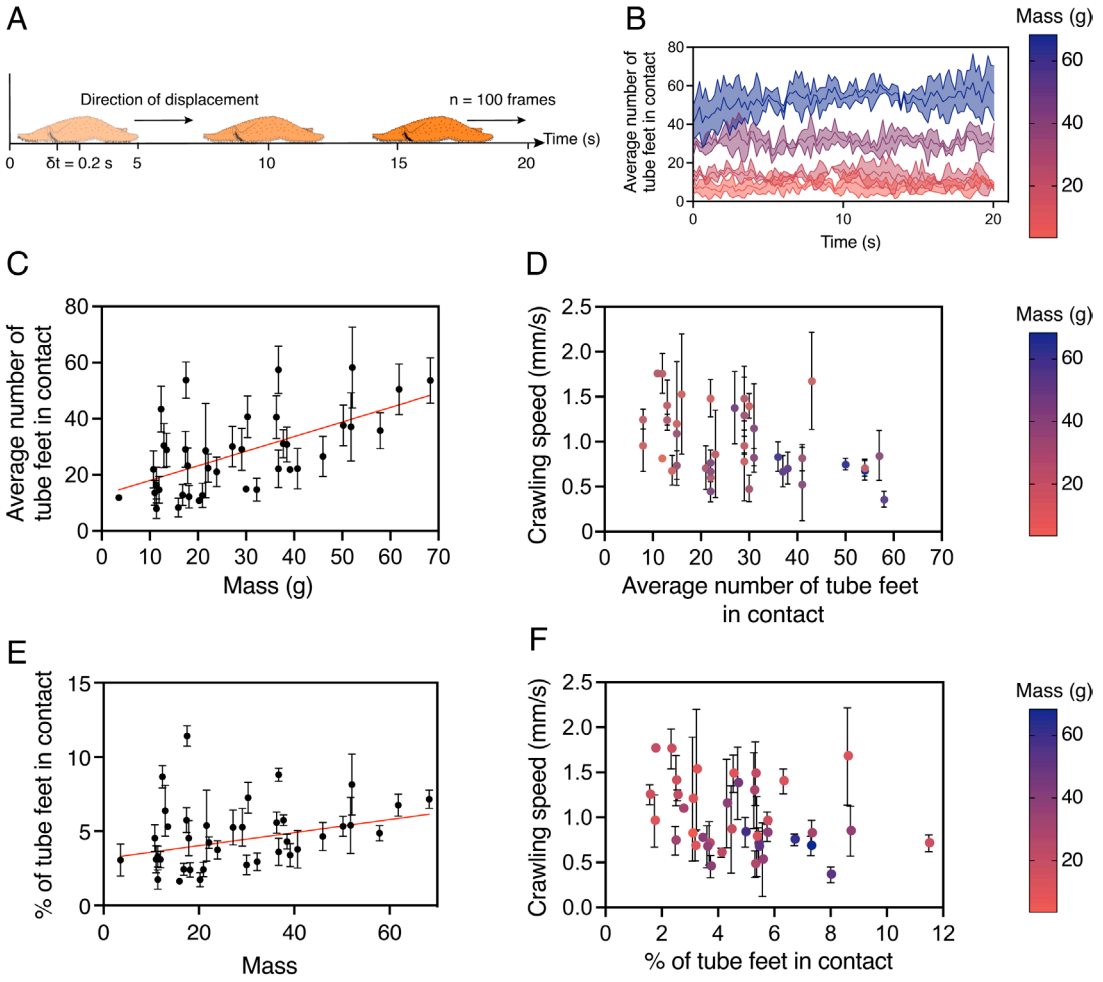


**Fig. 3.** Crawling speed in *A. rubens* is not affected by the number of adhering tube feet. (*A*) Displacement of *A. rubens* recorded over 20 s, with the number of tube feet in contact and the contact area measured every 0.2 s. (*B*) Average number of tube feet in contact over time for individuals of increasing mass (color-coded from light to dark: 11.39 g, 20.96 g, 37.75 g, and 68.31 g). (*C*) Relationship between the average number of tube feet in contact and body mass ($n$ = 39, $R^2$ = 0.3536, $P$ < 0.0001). (*D*) Crawling speed as a function of the average number of tube feet in contact and body mass ($n$ = 39). (*E*) Relationship between the percentage of tube feet in contact and body mass (n = 39, $R^2$ = 0.0926, $P$ = 0.0002). (*F*) Relationship between the crawling speed and the average percentage of tube feet in contact (n = 39). All data are presented as mean ± SD.

Analysis of the mean tube foot contact area during the adhesion stage shows a positive correlation with natural body mass (Fig. 4*C* and *SI Appendix*, Fig. 5*A*). In log–log space, the estimated slope was 0.42 (95 % CI 0.38 to 0.47) for *A. rubens* and 0.48 (95 % CI 0.44 to 0.53) for *M. glacialis*, indicating that contact area increases with mass but more slowly than expected under isometric scaling (slope = 0.66) (26). This negative allometry suggests that larger sea stars do not enlarge individual tube feet proportionally to body mass; instead, they likely enhance total adhesion by increasing the number of tube feet rather than their size. In addition, a weak but significant positive relationship was observed between contact time and contact area (Fig. 4*D*), indicating that larger tube feet require slightly longer contact times during locomotion.

We also found an inverse relationship between crawling speed and contact time (Fig. 4*E* and *SI Appendix*, Fig. 5*B*) demonstrating that longer contact times are associated with slower locomotion. This indicates that rapid detachment of tube feet is essential for achieving higher crawling speeds. Notably, contact times during locomotion remained below one minute, typically ranging from 3 to 20 s. Moreover, some tube feet appear to be reused during locomotion via repetitive detachment and attachment cycles, and the time between two successive adhesion stages is referred to as the recovery stroke phase (*SI Appendix*, Fig. 6*A*). This parameter remained relatively constant across individuals of different natural body masses, with an average duration of 18.6 ± 6.5 s (*SI Appendix*, Fig. 6*B*).

Taken together, these findings suggest that the relationship between body mass and crawling speed is mediated through adhesion dynamics. They highlight the pivotal role of tube feet coordination and timing in enabling adaptive and efficient locomotion in *A. rubens.*

**Dynamic Adjustments in Tube Foot Contact Time in Response to Mass Changes.** To validate these findings, we conducted perturbation experiments involving artificial mass alteration and inverted locomotion in *A. rubens.* In the first experiment, individuals were fitted with a 3D-printed backpack carrying additional weights equivalent to 25 or 50% of their body mass (Fig. 5*A* and Movie 6). The percentage of tube feet in contact with the substrate increased slightly but significantly with added load (Fig. 5*B*), although the overall fraction of engaged podia remained low (<10 %). This modest increase likely reflects a minor load-dependent recruitment of additional tube feet to enhance stability.

Despite this adjustment, instantaneous crawling speed declined significantly with added weight (Fig. 5*C*), likely due to the greater tube foot force required for tube foot detachment and propulsion.

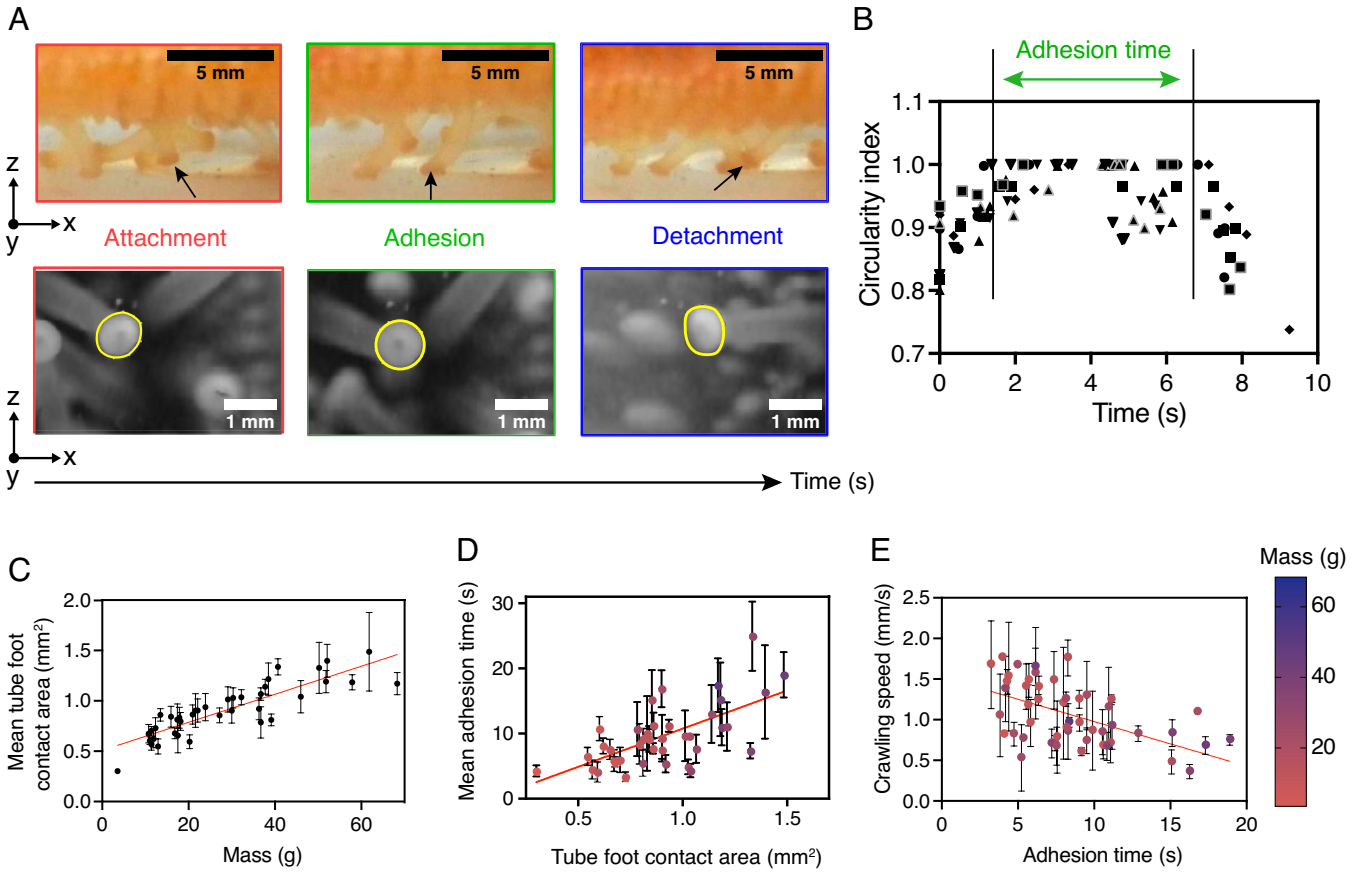


**Fig. 4.** Tube foot adhesion time correlates with sea star locomotion in *A. rubens*. (*A*) High-magnification imaging reveals the three stages of tube foot adhesion during locomotion. *Top* panels show side views of an individual in motion, while *Bottom* panels display views of the ambulacral groove. Adhesion time is defined as the duration of the adhesion stage. (*B*) Temporal variation in the circularity index of individual tube feet (n = 10). Vertical lines indicate the start and end of the adhesion phase. (*C*) Relationship between mean tube foot contact area and body mass (n = 39, $R^2 = 0.6203$, $P < 0.0001$). In log–log space, the slope is 0.42 (95 % CI 0.38 to 0.47), showing that contact area increases more slowly than predicted by isometry, consistent with negative allometry. (*D*) Relationship between mean adhesion time and tube foot contact area (n = 39, $R^2 = 0.3088$, $P < 0.0001$). (*E*) Crawling speed as a function of tube foot adhesion time (n = 49, $R^2 = 0.2115$, $P < 0.0001$). All data are presented as mean ± SD.

Correspondingly, adhesion time increased with mass, from 4.3 ± 1.4 s for the empty backpack to 5.9 ± 1.9 s and 8.4 ± 2.6 s for +25 and +50% mass, respectively (Fig. 5*D*). This prolongation likely reflects the increased propulsive force required to move the added weight during each locomotor cycle. It indicates that the main compensatory mechanism under increased mechanical demand is the modulation of adhesion duration rather than a change in the number of feet in contact.

**Biomechanics Model.** We hypothesized that the observed increase in contact time with increasing body mass is governed by the biomechanics of the tube feet. To corroborate this hypothesis, we employed a mathematical model of sea star locomotion driven by tube feet forces (3). In this model, the sea star is represented as a rigid body of mass $m$, whose center of mass is located at $(x, y)$ in the vertical plane. The ventral surface is lined by N tube feet, anchored at evenly spaced distance intervals $d$ along the sea star body (Fig. 5*E*). Each tube foot is characterized by its length $\ell$ and inclination angle $\theta$ from the vertical axis. When attached and engaged with the substrate, a tube foot exerts an active force $F_a$, caused by the activation of muscle tissues lining the stem and ampulla, and experiences a passive restorative force $F_p$ due to connective tissue resistance. Both active and passive forces act along the length of the tube foot and can either push or pull on the sea star's body, depending on which muscle group is activated: Ampullar muscle contraction extends the tube foot and produces a pushing force, while stem contraction shortens the foot, resulting in a pulling force (3, 5).

We imposed no direct control on the sea star center of mass and considered a fully decentralized adaptive control of the tube feet. Each attached tube foot senses its own length and inclination angle $(\ell, \theta)$ and responds accordingly. Depending on the sign of $\theta$, the tube foot experiences shear either in the same or opposite direction to its horizontal motion and decides to either push or pull, following a Hill's muscle model (Fig. 5*E*). When the tube foot is axially stretched beyond a critical length $\ell_{detach}$, it detaches. In the detached state, the tube foot applies no force and remains inactive for a stochastic time duration governed by a reattachment rate $\lambda$; the longer it remains detached, the higher its probability of reattaching. Upon reattachment, the tube foot makes a random step in the direction of the sea star's motion. A full mathematical description of the model is provided in the Theoretical *SI Appendix*. In the model, the characteristic length scale is set by the tube foot length, while the time scale is determined by the passive relaxation time of a foot returning to its resting length after deformation.

We examined numerically the sea star locomotion, while keeping all parameters the same, except for the sea star weight and detachment length. $\ell_{detach}$ Namely, we increased the sea star weight by 25 and 50%, consistent with our experiments, and correspondingly, increased $\ell_{detach}$ with increasing the sea star weight (Fig. 5*F* and Movie 7). For each weight, we performed 25 Monte-Carlo simulations, corresponding to random initial conditions of the

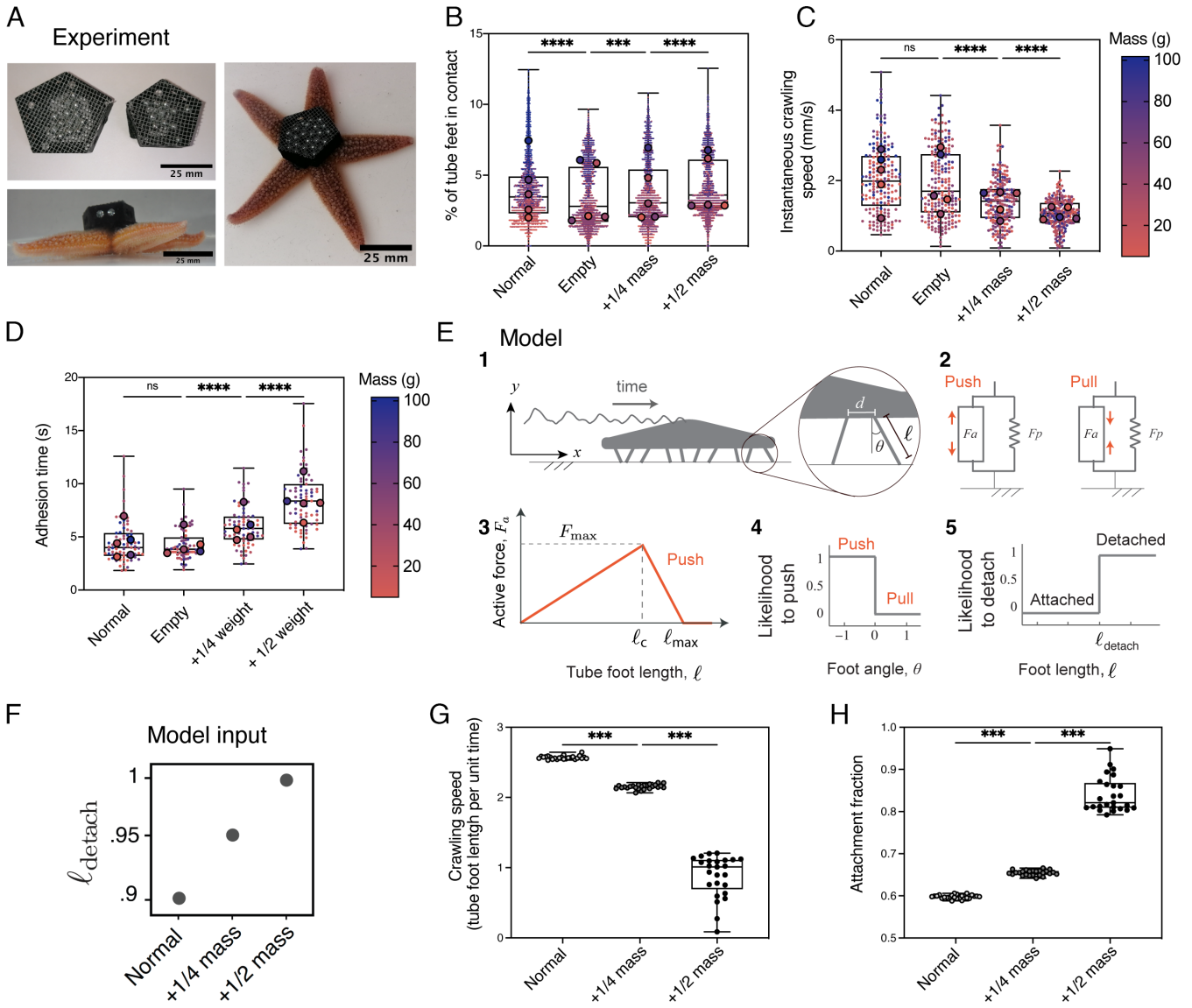


**Fig. 5.** Sea star locomotion dynamics in response to load changes are modulated by adhesion time in *A. rubens*. (*A*) Photographs showing two representative sizes of 3D-printed backpacks used to artificially increase the body mass by 25 and 50% with stainless steel beads. (*B*) Percentage of tube feet in contact with the substrate, (*C*) instantaneous crawling speed, and (*D*) tube foot adhesion time under four conditions: normal locomotion, empty backpack, +25% body mass, and +50% body mass (N = 5 sea stars per condition). Data in all superplots are color-coded by mass. Each small dot corresponds to a single tube foot contact event, and large dots indicate means per individual. Three replicates were performed per sea star. (*E*) Schematic of the biomechanical model used to simulate sea star locomotion through locally controlled tube feet. (1) Model organism propelled by 10 tube feet. The inset defines key parameters: tube foot length ($l$), tilt angle ($\theta$), and interfoot spacing ($d$). (2) Mechanical model of a single tube foot, composed of a passive linear spring and an active force generator capable of producing either pushing or pulling forces depending on muscle activation. (3) Active force profile based on Hill's muscle model. (4) Local control policies at the level of individual tube feet. These define the probability of transitions between pushing and pulling states and between attached and detached states, based on sensory feedback. (5) Tube feet detach when stretched beyond a threshold length $l_{detach}$. (*F*) The corresponding length of detachment for the tube feet are $l_{detach}$ = 0.9, 0.95, 1, respectively. Parameter values are $N$ =100, $L$ = 40, $l$ = 1, $F_{max}$ = 0.4, $\lambda$ = 5 (*G*) Simulated crawling speed and (*H*) attachment fraction $\tau$, with $\tau = \sum_{i=1}^{N} T_i^{attached}/NT$, defined as the sum over all tube feet of the time $T_i^{attached}$ each foot spends in attachment, divided by the total simulation time T times the number $N$ of tube feet. Both metrics are shown as a function of sea star mass, increasing from baseline to highest ($W$ = 2, 2.5, 3). For each mass condition, 25 simulations were performed with randomized initial foot states. ***$P$ < 0.001, ****$P$ < 0.0001, and ns = not significant.

tube feet. We calculated the crawling speed, defined as the total distance traveled by the center of mass divided by the total simulation time $T$. We also calculated the attachment fraction, $\tau = \sum_{i=1}^{N} T_i^{attached}/NT$, defined as the sum over all tube feet of the total time each foot spends in attachment $T_i^{attached}$, divided by $NT$. This gives the average proportion of time that a typical tube foot is attached. Interestingly, theoretical simulations of crawling speed (Fig. 5*G*) and attachment fraction (Fig. 5*H*) in response to mass variation show trends similar to those observed experimentally (Fig. 5 *C* and *D*), supporting the validity of our model based on fully decentralized adaptive control of the tube feet. These findings support the hypothesis that sea star locomotion can emerge from local sensing and mechanical feedback at the level of individual tube feet, without requiring centralized control. Moreover, they demonstrate that crawling speed under increased mechanical load can be modulated through local adaptation of detachment timing.

**Dynamic Adjustments in Tube Foot Adhesion Time in Inverted Setup.** In the second perturbation experiment, we placed each individual upside down and then we analyzed inverted locomotion (Fig. 6*A* and Movie 8), a condition that mimics the natural challenge of navigating vertical or overhanging surfaces in their environment (4).

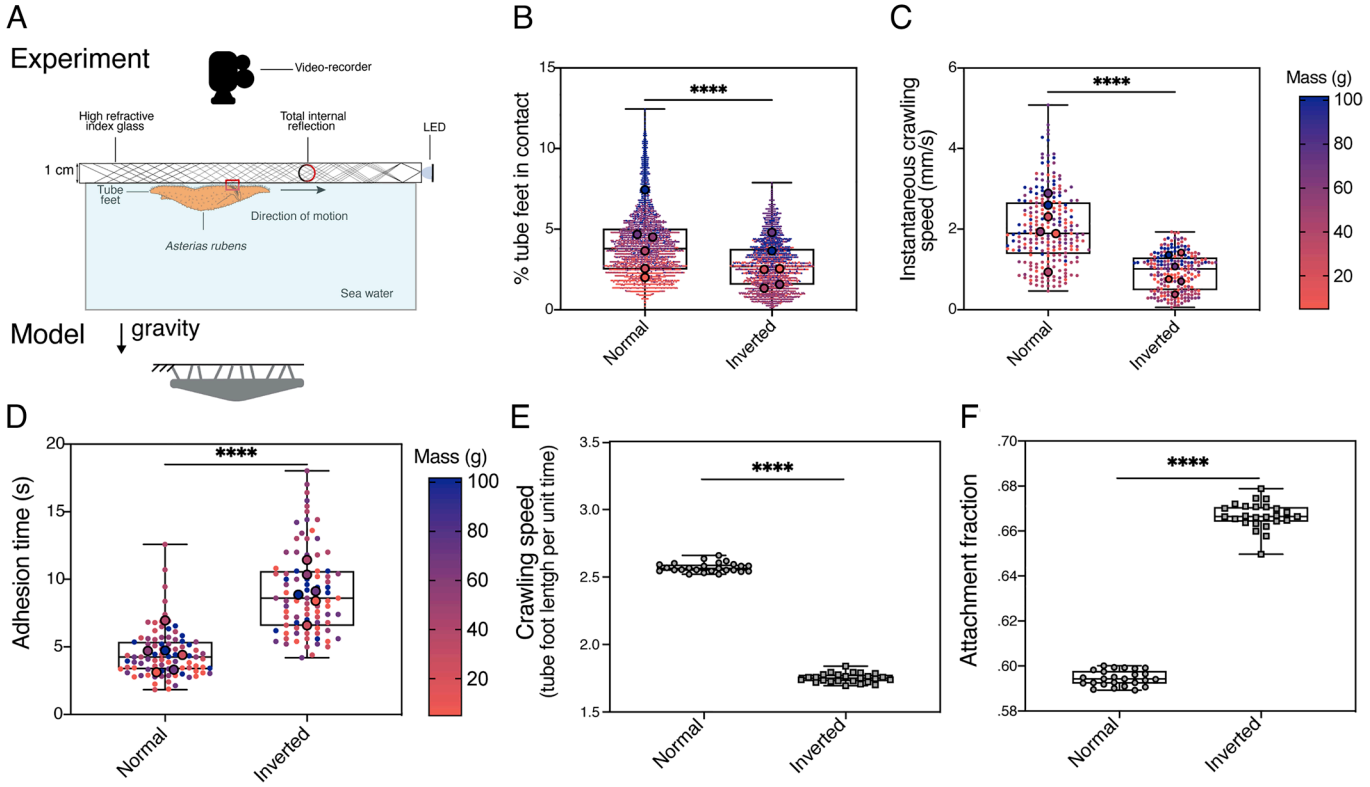


**Fig. 6.** Modulation of adhesion time enables *A. rubens* to adapt its locomotion under inverted conditions. (*A*) Schematic of the experimental setup for inverted locomotion. Sea stars were allowed to crawl upside down, while their oral surface was recorded from above using a camera positioned over the aquarium. (*B*) Percentage of tube feet in contact, (*C*) instantaneous crawling speed, and (*D*) tube foot adhesion time for normal versus inverted conditions (N = 6 sea stars per condition). All data are displayed as superplots, showing individual data points. Each dot corresponds to an individual contact event, and large dots indicate means per individual. Each individual was tested in three replicates. (*E*) Simulated crawling speed and (*F*) attachment fraction $\tau = \sum_{i=1}^{N} T_i^{attached}/NT$, defined as the sum over all tube feet of the time $T_i^{attached}$ each foot spends in attachment, divided by the total simulation time T times the number N of tube feet. Both shown for the flat and inverted sea stars. For each orientation, 25 random simulations have been performed. Parameter values are N = 100, L = 40, l = 1, $F_{max} = 0.4$, $\lambda = 5$, with no parameter adjustment between normal and inverted simulations. ****$P < 0.0001$.

This inversion alters the distribution of gravitational forces, effectively increasing the load on the tube feet as they counteract the downward pull, thereby requiring greater adhesive forces and coordination to maintain stability and locomotion. The mean percentage of tube feet in contact slightly decreased in the inverted position compared to the normal condition (Fig. 6*B*), suggesting a compensatory response to counteract the effect of gravity and maintain stability. Interestingly, instantaneous crawling speed was significantly reduced in the inverted condition (Fig. 6*C*), likely due to the higher energy demands associated with this altered posture. Adhesion time was also significantly prolonged during inverted locomotion (Fig. 6*D*), consistent with the need for stronger adhesion to prevent detachment under gravity. The consistency between experimental observations and simulations indicates that these changes in tube foot behavior arise from the passive mechanical dynamics of the decentralized system rather than from an active compensatory response.

We compared numerically, in the context of our model, sea star locomotion under normal and inverted conditions, with no adjustment of parameters, keeping all parameters constant (Movie 9). Again, for each condition, we performed 25 Monte-Carlo simulations, corresponding to random initial conditions of the tube feet, and calculated the crawling speed and attachment fraction, $\tau = \sum_{i=1}^{N} T_i^{\text{attached}}/NT$. The simulation results show trends similar to those observed experimentally (Fig. 6 *E* and *F*), confirming the validity of the biomechanical approach.

Together, these perturbation experiments demonstrate that sea stars employ dynamic adjustments in tube foot adhesion time to adapt to increased mechanical demands, whether due to added weight or altered locomotion modes. These experimental findings, combined with the modeling results, underscore the critical role of tube feet dynamics in stabilizing and adapting sea star locomotion under varying physical constraints.

## Discussion

While the biomechanics of tube feet has been described in echinoderms, the dynamics of their contact formation and breakage during locomotion and the number of tube feet involved in movement have remained largely unexplored. Unlike many animals, sea stars display a less straightforward relationship between body mass and crawling speed (16, 20, 22, 27), prompting the need for a deeper examination of the mechanisms underlying their locomotion, especially by focusing on the role of their tube feet (16).

Our study demonstrates that *A. rubens* maintains pentaradial symmetry across a wide size range. The observed morphological consistency, along with only minimal angular deviations between arms, likely reflects evolutionary pressures to preserve efficient, symmetrical locomotion (3, 4). This robust geometry may support coordinated activation of tube feet and enhance mechanical stability during movement.

Although environmental factors, such as temperature, flow conditions, and substrate inclination are known to influence echinoderm locomotion (16, 22, 27, 28), our results show that the average crawling speed of *A. rubens*, 0.98 ± 0.38 mm/s, is

consistent with previous studies (29), validating our experimental design. Surprisingly, we found that crawling speed is not correlated with the average number or percentage of tube feet in contact with the substrate. Even though larger individuals naturally possess more tube feet, the proportion actively engaged in adhesion increases slightly with body mass but remains low (< 10 %). This subtle adjustment likely contributes to maintaining stability in larger animals, yet it is insufficient to account for the observed mechanical adaptation, which primarily arises from changes in adhesion time. The lack of dependence on contact area further underscores an evolutionary adaptation that enables sea stars to maintain consistent and efficient locomotion across a variety of surfaces and environmental conditions. For instance, in *Acanthaster solaris*, locomotion speed is influenced by substrate texture, with slower movement observed on rougher surfaces (27). In *Patiria miniata*, individuals can possess five or six arms, yet the number of arms has been shown to have no significant effect on crawling speed (16). Additionally, comparisons across species indicate that sea stars inhabiting tropical environments generally exhibit faster locomotion than those from temperate regions (16).

Our observation highlights the importance of tube foot adhesion timing over mere contact number. Video recordings with a high pixel count revealed that locomotion consists of a cyclic sequence of attachment, adhesion, and detachment phases. While larger tube feet and greater contact areas likely enhance adhesion force, they also lead to increased adhesion time, which in turn reduces crawling speed. These findings reveal a trade-off between adhesive performance and locomotor efficiency: Rapid movement requires shorter adhesion times and thus faster detachment–reattachment cycles. A positive correlation between stride frequency and maximum speed has been described in several animals using dynamic adhesion for locomotion (30, 31).

Perturbation experiments show that *A. rubens* dynamically modulates tube foot contact time in response to added load. The number of adhering tube feet slightly increased and, most importantly, crawling speed decreased and contact time increased proportionally with the added weight. This suggests that sea stars rely on local mechanical feedback to adaptively tune tube feet dynamics, without requiring changes in coordination or overall foot engagement. Notably, these same patterns were observed under inverted locomotion, where gravitational forces were altered, although in this case the percentage of tube feet in contact decreased slightly. The similarity of behavioral responses across both perturbations, additional mass and inversion, indicates a conserved mechanical strategy to stabilize movement under changing physical conditions.

Numerical simulations based on a biomechanical model of tube foot function replicated the observed trends. By varying body mass and detachment thresholds, the model reproduced the inverse relationship between crawling speed and adhesion time. The simulations further demonstrated that local sensing and adaptive control at the level of individual tube feet are sufficient to generate coherent and efficient crawling behavior, without centralized control. However, a centralized coordination in stepping direction appears necessary for efficient locomotion (32, 33).

Mechanisms of adaptation may differ between gaits, however. Our work complements previous studies on sea star locomotion (4, 5, 33), which focused on the bouncing gait observed in some other species. In contrast, the present work examines the crawling gait of *A. rubens*, where the number of tube feet engaged remains nearly constant while adhesion time increases under load. Both the bouncing and crawling gaits therefore illustrate distinct mechanical strategies for coping with increased body weight, either by recruiting more tube feet or by prolonging contact duration, yet in both cases locomotor adaptation emerges through decentralized, mechanically mediated control at the level of individual tube feet. This gait-dependent distinction refines our understanding of cooperative transport in sea stars across scales and species.

Together, our findings identify tube foot adhesion time as a key, mass-dependent parameter governing sea star locomotion. This mechanism provides a flexible strategy to balance stability and speed across individuals and environmental conditions. By demonstrating that adaptive locomotion can arise from purely local mechanical feedback, without a central pattern generator, our work reveals a decentralized control principle in a brainless organism. Such distributed control, rooted in local sensing and mechanical coupling among tube feet, allows sea stars to maintain robust and adaptive movement under diverse physical constraints.

FTIR-based imaging has been previously developed to measure contact areas of adhesive pads during locomotion, but it has mostly been applied to studies of tree frog climbing, stress distribution in gecko toes (34–36), and insect adhesion (37–39). Our FTIR platform offers a promising avenue for investigating locomotion dynamics in echinoderms and other soft-bodied aquatic animals. Beyond its biological relevance, this insight highlights general design principles for soft and multicontact robotic systems, in which coordinated motion can emerge spontaneously from the interplay between structure and mechanics rather than from explicit centralized control.

## Conclusion

This study demonstrates that *A. rubens* modulates tube foot adhesion time to maintain effective locomotion across a range of body sizes and mechanical challenges. By combining high-resolution imaging, perturbation experiments, and biophysical modeling, we show that adhesion time, rather than the number of contacting tube feet, is the principal determinant of crawling speed. These results reveal a decentralized, mechanically adaptive strategy that enables robust and versatile locomotion in sea stars.

## Materials and Methods

**Collection and Maintenance of Sea Stars.** Specimens of *A. rubens* Linnaeus, 1758, were hand-collected at low tide on breakwaters at Knokke-Heist, Belgium. Specimens of *Marthasterias glacialis* (Linnaeus, 1758) were hand-collected at the Concarneau marine station, France during low tide. They were brought back to the University of Mons, where they were housed in recirculating seawater aquaria maintained at a temperature of 12 to 13 °C and a salinity of 30 to 33 psu. Salinity was controlled using a precision salinity refractometer (ATC-S/Mill-E, ±0.2%). The sea stars were fed weekly with fresh mussels (*Mytilus edulis* L.). The collected individuals ranged in size from 60 mm to 180 mm in total diameter (Fig. 1*B*). To minimize stress and allow for acclimatization, all individuals were kept under these conditions for at least two weeks prior to conducting locomotion trials. Some of the specimens used in the experiments shown in Fig. 1*A* were kindly provided by the aquariology department of Nausicaá (Boulogne-sur-Mer, France).

**Morphometric Analysis.** To assess the size and morphological parameters of *A. rubens*, high-resolution images of the oral surface were taken in seawater before each experiment using a Nikon 1J5 camera equipped with a 1 Nikkor 10-30 VR lens. Videos and images were analyzed using Fiji (40). To measure the mass of each sea star, the oral surface was gently dried with a paper towel, and the specimen was weighed on a digital balance inside a beaker full of seawater. To determine the numbers of tube feet per arm, individuals were anesthetized in a 3.5% solution of magnesium chloride in seawater for ten minutes to relax their tube feet. Then, three arms were randomly selected, and the number of tube feet was counted to provide representative data on tube foot distribution.

**Measurements for Locomotion Experiments.** Locomotion trials were conducted in an experimental glass aquarium, where seawater temperature was maintained at 15 °C and salinity was set to 33 psu. The oral surface of *A. rubens* was video recorded using a Nikon 1J5 camera with a Nikkor 10–30 VR lens positioned beneath the aquarium. Each sea star was carefully placed at the bottom center of the aquarium, and its movement was recorded for 20 seconds once it began crawling. Measurements for locomotion assays included locomotion speed, the number of tube feet in contact with the substrate and the contact area during the locomotion. The percentage of tube feet in contact during locomotion was calculated for each individual using the following formula:

$$\frac{\text{Number of tube feet in contact}}{\text{Total number of tube feet}} \times 100 = \text{Percentage of tube feet in contact.}$$

The instantaneous locomotion speed was calculated by dividing the displacement by the time required to move between two points. The displacement D between two successive positions $(x_1, y_1)$ and $(x_2, y_2)$ was determined using the following equation:

$$\sqrt{(x_2 - x_1)^2 + (y_2 - y_1)^2} = D.$$

The dynamics of tube foot adhesion was analyzed by recording high-magnification videos of the oral surface of *A. rubens* during locomotion. These videos were captured using a Nikon D90 camera equipped with an AF-S Nikkor 105 mm lens. For these recordings, tube foot adhesion time and contact area were precisely measured, providing detailed insights into adhesion dynamics.

**Perturbation Experiments.** Backpacks were 3D-printed using an Ultimaker printer with PLA filament. The backpacks were securely attached to the sea stars using veterinary glue (Vetbond, 3M Deutschland GmbH) (Fig. 5*A*). Locomotion was recorded under three conditions: with an empty backpack and with additional weights equivalent to 25 and 50% of the sea star's body mass. For each condition, movements were recorded for 20 s under the same setup as the experiments without backpacks. Stainless-steel marbles were used to provide the additional mass. In the inverted locomotion experiments, individuals of *A. rubens* were allowed to walk upside down on a high refractive index glass plate equipped with an FTIR-based system (Fig. 6*A*). Locomotion was recorded using a Nikon 1J5 camera with a Nikkor 10–30 VR lens positioned above the plate to visualize their altered movement during inverted locomotion.

**Statistical Analysis.** All experiments were performed on $N = 5$ to 6 individual sea stars, each tested successively under the different experimental conditions. For each individual and condition, measurements were obtained from $n \approx 15$ tube feet, which represent subsamples nested within individuals. To account for this hierarchical structure and repeated measurements, data were analyzed using mixed-effects models (restricted maximum likelihood, REML) implemented in Prism 10.0 (GraphPad Software). In these models, condition was treated as a fixed effect and individual as a random effect, allowing each sea star to serve as its own control while preserving independence of observations.

Prior to analysis, data distributions were assessed for normality using the D'Agostino–Pearson omnibus test, which combines skewness and kurtosis statistics. When normality assumptions were not met, nonparametric tests were applied (Mann–Whitney for two-group comparisons; Kruskal–Wallis followed by Dunn's multiple-comparison test for more than two groups). For parametric mixed-effects analyses, Geisser–Greenhouse corrections were applied when sphericity was violated, and Holm–Šidák post hoc adjustments were used to control for family-wise type I error ($\alpha = 0.05$).

To ensure robustness and avoid potential pseudoreplication related to repeated measurements of tube feet within individuals, complementary analyses were performed on per-individual mean values (i.e., the average of 15 podia per condition). Both analytical approaches yielded consistent significance patterns, confirming that the observed effects are independent of the statistical treatment and unaffected by the nested sampling structure.

For comparisons of crawling speed across substrates, individual body mass was included as a covariate in a linear model, which confirmed that substrate effects were independent of size ($P = 0.27$). Linear regressions were used to analyze allometric scaling (e.g., arm length, contact area, or crawling speed versus body mass), and slopes with their 95 % CI were reported to assess deviations from theoretical isometry.

Unless otherwise stated, data are expressed as mean ± SD. A 95 % CI was used for all analyses, and detailed statistical parameters are provided in the corresponding figure captions: $*P < 0.05$, $**P < 0.01$, $***P < 0.001$, $****P < 0.0001$, and n.s. is not significant.

**Data, Materials, and Software Availability.** All study data are included in the article and/or supporting information.

**ACKNOWLEDGMENTS.** A.D., P.F., and S.N.G. acknowledge funding from the University of Mons–UMONS, the Research Institute for Biosciences Project Starlight, FEDER Prostem Research Project no. 1510614 (Wallonia DG06), the F.R.S.-FNRS Epiforce Project no. T.0092.21, the F.R.S.-FNRS In the footsteps of sea stars Project no. T.0088.20, the F.R.S.-FNRS Cellsqueezer Project no. J.0061.23, the F.R.S.-FNRS Optopattern Project no. U.NO26.22, and the Interreg projects MICROPLAITE and ANTIRESI, which are financially supported by Interreg France-Wallonie-Vlaanderen (Fonds Européen de Développement Régional, FEDER-ERDF). A.D. is financially supported by F.R.S.-FNRS as FRIA Grantee. S.N.G. acknowledges le Fonds pour la Recherche Médicale dans le Hainaut (FRMH). P.F. is Research Director of the F.R.S.-FNRS. We thank Stéphane Hénard, Renaud Herbert, and Denis Tirmarche from the Aquariology Department of Nausicaá (Boulogne-sur-Mer, France) for kindly providing access to various sea star species. We thank Matthew McHenry for his valuable input in this manuscript and Philippe Dubois for his constructive comments on the statistical analyses.

Author affiliations: [a]SYMBIOSE Lab, Research Institute for Biosciences, CIRMAP, University of Mons—UMONS, Mons B-7000, Belgium; [b]Biology of Marine Organisms and Biomimetics Unit, Research Institute for Biosciences, University of Mons—UMONS, Mons B-7000, Belgium; [c]Mechanical Engineering, California State University, Northridge, CA 91330; [d]Aerospace and Mechanical Engineering, University of Southern California, Los Angeles, CA 90089; [e]Functional Morphology and Biomechanics, Zoological Institute, Kiel University, Kiel D-24118, Germany; and [f]Physics and Astronomy, University of Southern California, Los Angeles, CA 90089

1. J. E. Smith, The activities of the tube feet of *Asterias rubens* L: I. The mechanics of movement and of posture. *J. Cell Sci.* **88**, 1–14 (1947).
2. J. M. Lawrence, *A Functional Biology of Echinoderms* (Funct. Biol. Ser. Croom Helm, London, 1987).
3. S. Heydari, A. Johnson, O. Ellers, M. J. McHenry, E. Kanso, Sea star inspired crawling and bouncing. *J. R. Soc. Interface* **17**, 20190700 (2020).
4. T. Po, E. Kanso, M. J. McHenry, Cooperative transport in sea star locomotion. *Curr. Biol.* **34**, 2551–2557.e4 (2024).
5. O. Ellers *et al.*, Soft skeletons transmit force with variable gearing. *J. Exp. Biol.* **227**, jeb246901 (2024).
6. R. Santos, S. Gorb, V. Jamar, P. Flammang, Adhesion of echinoderm tube feet to rough surfaces. *J. Exp. Biol.* **208**, 2555–2567 (2005).
7. E. Hennebert *et al.*, Sea star tenacity mediated by a protein that fragments, then aggregates. *Proc. Natl. Acad. Sci.* **111**, 6317–6322 (2014).
8. P. Flammang, C. De Ridder, M. Jangoux, Ultrastructure of the penicillate podia of the spatangoid echinoid *Echinocardium cordatum* (Echinodermata) with special emphasis on the epidermal sensory-secretory complexes. *Acta Zool.* **72**, 151–158 (1991).
9. P. Flammang, A. Michel, A. V. Cauwenberge, H. Alexandre, M. Jangoux, A study of the temporary adhesion of the podia in the sea star *Asterias rubens* (Echinodermata, Asteroidea) through their footprints. *J. Exp. Biol.* **201**, 2383–2395 (1998).
10. C. O. Hermans, The duo-gland adhesive system. *Oceanogr. Mar. Biol.* **21**, 283–339 (1983).
11. M. Algrain *et al.*, In the footsteps of sea stars: Deciphering the catalogue of proteins involved in underwater temporary adhesion. *Open Biol.* **12**, 220103 (2022).
12. J. E. Smith, The mechanics and innervation of the starfish tube foot-ampulla system. *Philos. Trans. R. Soc. Lond. B Biol. Sci.* **232**, 279–310 (1946).
13. E. Hennebert, D. Haesaerts, P. Dubois, P. Flammang, Evaluation of the different forces brought into play during tube foot activities in sea stars. *J. Exp. Biol.* **213**, 1162–1174 (2010).
14. R. S. McCurley, W. M. Kier, The functional morphology of starfish tube feet: The role of a crossed-fiber helical array in movement. *Biol. Bull.* **188**, 197–209 (1995).
15. J. E. Smith, The role of the nervous system in some activities of starfishes. *Biol. Rev.* **20**, 29–43 (1945).
16. E. M. Montgomery, A. R. Palmer, Effects of body size and shape on locomotion in the bat star (*Patiria miniata*). *Biol. Bull.* **222**, 222–232 (2012).
17. H. S. Jennings, "Behavior of the Starfish Asterias forreri de Loriol" in *Zoology*, (University Of California Publications, ed. 2, 1907), pp. 53–187.
18. L. J. Cole, Direction of locomotion of the starfish (*Asterias forbesi*). *J. Exp. Zool.* **14**, 1–32 (1913).
19. Richard C. Brusca, Gary J. Brusca, *Invertebrates* (Sinauer Associates, ed. 2, 2003).
20. E. M. Montgomery, Predicting crawling speed relative to mass in sea stars. *J. Exp. Mar. Biol. Ecol.* **458**, 27–33 (2014).

21. M. R. Hirt, W. Jetz, B. C. Rall, U. Brose, A general scaling law reveals why the largest animals are not the fastest. *Nat. Ecol. Evol.* **1**, 1116–1122 (2017).
22. B. Mueller, A. Bos, G. Graf, G. Gumanao, Size-specific locomotion rate and movement pattern of four common Indo-Pacific sea stars (Echinodermata; Asteroidea). *Aquat. Biol.* **12**, 157–164 (2011).
23. R. J. Full, M. S. Tu, Mechanics of a rapid running insect: Two-, four-and six-legged locomotion. *J. Exp. Biol.* **156**, 215–231 (1991).
24. T. Weihmann, The smooth transition from many-legged to bipedal locomotion–Gradual leg force reduction and its impact on total ground reaction forces, body dynamics and gait transitions. *Front. Bioeng. Biotechnol.* **9**, 769684 (2022).
25. D. Labonte, W. Federle, Scaling and biomechanics of surface attachment in climbing animals. *Philos. Trans. R. Soc. Lond. B Biol. Sci.* **370**, 20140027 (2015).
26. D. Labonte *et al.*, Extreme positive allometry of animal adhesive pads and the size limits of adhesion-based climbing. *Proc. Natl. Acad. Sci.* **113**, 1297–1302 (2016).
27. M. S. Pratchett *et al.*, Body size and substrate type modulate movement by the western Pacific crown-of-thorns starfish. *Acanthaster solaris*. *PLOS ONE* **12**, 1–14 (2017).
28. A. P. St-Pierre, P. Gagnon, Wave action and starvation modulate intra-annual variation in displacement, microhabitat selection, and ability to contact prey in the common sea star, Asterias rubens Linnaeus. *J. Exp. Mar. Biol. Ecol.* **13**, 95–107 (2015).
29. P. Mayo, A. M. Mackie, Studies of avoidance reactions in several species of predatory British seastars (Echinodermata: Asteroidea). *Mar. Biol.* **38**, 41–49 (1976).
30. W. Federle, D. Labonte, Dynamic biological adhesion: Mechanisms for controlling attachment during locomotion. *B Biol. Sci.* **374**, 20190199 (2019).
31. T. E. Higham, Frictional adhesion of geckos predicts maximum running performance in nature. *J. Exp. Biol.* **228**, jeb247906 (2025).
32. G. A. Kerkut, The mechanisms of coordination of the starfish tube feet. *Behaviour* **6**, 206–232 (1954).
33. T. Po, L. Korob, M. J. McHenry, The directional control of phototaxis in sea stars (*Protoreaster nodosus*). *J. Exp. Biol.* **228**, jeb249293 (2025).
34. I. D. C. Hill *et al.*, The biomechanics of tree frogs climbing curved surfaces: A gripping problem. *J. Exp. Biol.* **221**, jeb.168179 (2018), 10.1242/jeb.168179.
35. E. V. Eason *et al.*, Stress distribution and contact area measurements of a gecko toe using a high-resolution tactile sensor. *Bioinspir. Biomim.* **10**, 016013 (2015).
36. N. S. Poulter, W. T. E. Pitkeathly, P. J. Smith, J. Z. Rappoport, "The physical basis of total internal reflection fluorescence (TIRF) microscopy and its cellular applications" in *Advanced Fluorescence Microscopy, Methods in Molecular Biology*, P. J. Verveer, Ed. (Springer, New York, 2015), pp. 1–23.
37. C. J. Clemente, W. Federle, Pushing versus pulling: Division of labour between tarsal attachment pads in cockroaches. *Proc. R. Soc. B Biol. Sci.* **275**, 1329–1336 (2008).
38. J.-H. Dirks, C. J. Clemente, W. Federle, Insect tricks: Two-phasic foot pad secretion prevents slipping. *J. R. Soc. Interface* **7**, 587–593 (2010).
39. C. J. Clemente *et al.*, Jumping without slipping: Leafhoppers (Hemiptera: Cicadellidae) possess special tarsal structures for jumping from smooth surfaces. *J. R. Soc. Interface* **14**, 20170022 (2017).
40. C. A. Schneider, W. S. Rasband, K. W. Eliceiri, NIH image to ImageJ: 25 years of image analysis. *Nat. Methods* **9**, 671–675 (2012).